A separate set of experiments in which oxygen was introduced to the gas phase at a rate comparable to $I/2F$, instead of electrochemically, gave practically the same results as those depicted in Figs. 2 to 4. Substituting Ag with the Sm_2O_3-CaO-Ag cermet or substituting YSZ with α-Al_2O_3 as the cermet support gave only marginal differences with respect to the results presented in Figs. 2 to 4. Consequently, the amount of Sm_2O_3 added to Ag and the nature of the support do not play any important role in the observed behavior. Decreasing the gas recirculation flow rate from 220 to 50 cm^3/min at STP does not affect the reactor performance. By further lowering the recirculation flow rate, there is a gradual loss in C_2 and ethylene selectivity and yield.

The improvement in C_2 selectivity and yield of the present work is not attributable to the properties of the Ag catalyst, which is in fact inferior to most state-of-the-art catalysts and gives yields per pass less than 3% (Fig. 5), but is a result of the reactor design. Also, periodic unsteady-state reactor operation gives higher performance than steady-state reactor operation (Fig. 5), although industrial practice favors, in general, the latter mode of operation. Optimization could lead to further improvements in yields.

Our gas recycle reactor is simpler than and substantially different from the simulated countercurrent moving bed of Aris and co-workers (10) and has led to high values of C_2 yield and a pronounced enhancement in ethylene yield. The underlying idea is, however, very similar: protection of the highly reactive desired products by means of selective adsorption. The same type of reactor could also be used for other potential uses of methane, such as partial oxidation to methanol or formaldehyde (or both), by means of an appropriate choice of the catalytic and adsorbent material.

REFERENCES AND NOTES

1. L. L. Hegedus *et al.*, *Catalyst Design: Progress and Perspectives* (Wiley, New York, 1987), pp. 1–10.
2. G. E. Keller and M. M. Bhasin, *J. Catal.* **73**, 9 (1982).
3. W. Hinsen and M. Baerns, *Chem. Ztg.* **107**, 223 (1983).
4. T. Ito and J. H. Lunsford, *Nature* **314**, 721 (1985).
5. J. S. Lee and S. T. Oyama, *Catal. Rev. Sci. Eng.* **30**, 249 (1988).
6. K. Otsuka, K. Suga, I. Yamanaka, *Catal. Today* **6**, 587 (1990).
7. D. Eng and M. Stoukides, *Catal. Rev. Sci. Eng.* **33**, 375 (1991).
8. J. H. Lunsford, *Catal. Today* **6**, 235 (1990).
9. P. Tsiakaras and C. G. Vayenas, *J. Catal.* **144**, 333 (1993).
10. A. L. Tonkovich, R. W. Carr, R. Aris, *Science* **262**, 221 (1993), and references therein.
11. C. G. Vayenas, S. Bebelis, S. Ladas, *Nature* **343**, 625 (1990).
12. C. G. Vayenas, S. Bebelis, I. V. Yentekakis, H.-G. Lintz, *Catal. Today* **11**, 303 (1992).
13. C. G. Vayenas and R. D. Farr, *Science* **208**, 593 (1980).
14. We thank the EEC Joule Programme for partial financial support, D. Sutija for preparing the Sm_2O_3-CaO powder, and our reviewers for helpful suggestions.

8 February 1994; accepted 25 April 1994

Control of Structure and Growth of Polymorphic Crystalline Thin Films of Amphiphilic Molecules on Liquid Surfaces

Susan P. Weinbach, Kristian Kjaer, Wim G. Bouwman,
Gerhard Grübel, Jean-François Legrand, Jens Als-Nielsen,
Meir Lahav, Leslie Leiserowitz

The spontaneous formation and coexistence of crystalline polymorphic trilayer domains in amphiphilic films at air-liquid interfaces is demonstrated by grazing incidence synchrotron x-ray diffraction. These polymorphic crystallites may serve as models for the early stages of crystal nucleation and growth, helping to elucidate the manner in which additives influence the progress of crystal nucleation, growth, and polymorphism and suggesting ways of selectively generating and controlling multilayers on liquid surfaces. Auxiliary molecules have been designed to selectively inhibit development of the polymorphs, leading primarily to a single phase monolayer.

The ability to engineer three-dimensional (3D) crystals and crystalline thin films by control of polymorphism is important in applications ranging from the bioavailability of drugs to the design of materials for electronics. Such control requires an understanding of the mechanism by which molecules in a supersaturated solution assemble to form ordered aggregates or nuclei. Our knowledge of the structure and dynamics of such nuclei has, in general, been inferred from the structure of the observed crystals, which correspond to the thermodynamically most stable form or forms of the extended lattice (1). Additives may be designed to bind specifically to the surfaces of particular polymorphs and so inhibit their achieving the critical size for nucleation, allowing a desired phase to grow without competition. This method has been used for the separation of enantiomers by crystallization (1, 2) and for the growth of single crystals of metastable polymorphs, including polar crystals for nonlinear optics (3). Here we report the spontaneous formation of coexisting "polymorphic" trilayers and monolayers at the air-liquid interface and make use of auxiliary molecules to influence their thickness and crystalline structure. These amphiphilic films, which can be directly monitored by grazing incidence x-ray diffraction (GID) (4–6) and specular x-ray reflectivity (6, 7), may serve as models for understanding the early stages of crystal nucleation and growth on the molecular level.

When spread on liquid water at surface pressure $\pi = 0$, arachidamide ($C_{19}H_{39}$-$CONH_2$) forms a monolayer with the molecules tilted by about 18° from the normal to the liquid surface, with two molecules in a rectangular unit cell of dimensions $a = 4.69$ Å and $b = 8.69$ Å (8). When spread on formamide or formamide-water subphases, however, two trilayer phases are formed, with the relative ratio between them varying with time. The formation of multilayers and the coexistence of more than one crystalline form provide a system for study of the selective growth of crystallites at the liquid interface. We have therefore designed auxiliary molecules that may influence the mode of crystallinity.

The GID measurements were conducted on liquid surface diffractometers at the undulator beamlines BW1 at HASYLAB, Deutsches Elektronen-Synchrotron (DESY) (Hamburg, Germany) and Troika, European Synchrotron Radiation Facility (ESRF) (Grenoble, France). The amphiphiles (9) were spread at room temperature, with mean molecular area of 24 $Å^2$ (calculated assuming coverage by a monolayer only) and $\pi = 0$, on the liquid surface in a Langmuir trough mounted on the diffractometer before the subphase was cooled to 5°C. In all systems, the molecules spontaneously formed highly crystalline films with corre-

---

S. P. Weinbach, M. Lahav, L. Leiserowitz, Department of Materials and Interfaces, Weizmann Institute of Science, 76100 Rehovot, Israel.
K. Kjaer and W. G. Bouwman, Physics Department, Risø National Laboratory, DK4000 Roskilde, Denmark.
G. Grübel and J.-F. Legrand, Experiments Division, European Synchrotron Radiation Facility, Grenoble, France.
J. Als-Nielsen, Physics Department, Risø National Laboratory, DK4000 Roskilde, Denmark, and Experiments Division, European Synchrotron Radiation Facility, Grenoble, France.

lation lengths (*10, 11*) of ≥1000 Å.

We first discuss pure arachidamide in the absence of auxiliary molecules. The GID patterns for arachidamide on formamide or on 70 mole percent (84% v/v) formamide-water subphase are given in Fig. 1A. The positions of the Bragg peaks, shapes of the associated Bragg rods, and x-ray reflectivity curves for films on the two different subphases are nearly identical. Figure 1B shows the intensity distribution of the diffraction pattern on formamide-water subphase as a function of both the horizontal (q_{xy}) and vertical (q_z) scattering vectors. The thickness of the films was deduced from the q_z width of the associated Bragg rods (Fig. 2) (*12–14*) and by specular x-ray reflectivity (Fig. 3) (*15, 16*). The full width at half maximum (FWHM) of the various Bragg rods (Fig. 2) averages to 0.09 $Å^{-1}$ for pure arachidamide, which corresponds to a film thickness of about 70 Å (*12*). The approximate length of an arachidamide molecule is 24 Å; thus, we may deduce that the film is essentially a trilayer. This is reasonable in terms of the requirement that the molecules form centrosymmetric hydrogen-bonded dimers and that the film surface exposed to the subphase should be hydrophilic and the surface exposed to the atmosphere be hydrophobic (Fig. 4). It is possible that the two upper layers of the trilayer need not have full occupancy with respect to the lowest layer; and thus, the apparent thickness of the film is an average over all domains.

Comparison of the GID patterns on the 100% and the 70% formamide subphases (Fig. 1A) reveals a constant ratio for the integrated intensities of the reflections at q_{xy} = 1.38, 1.61, and 1.68 $Å^{-1}$ and another constant ratio of the intensities for the reflections at q_{xy} = 1.53 and 1.69 $Å^{-1}$. This led to the idea that the first set of reflections correspond to one phase of a trilayer and that the other set corresponds to a second trilayer phase. The relative amount of the two phases depends on which subphase is used, and it also changes with time (Fig. 5).

The two reflections at q_{xy} = 1.53 and 1.69 $Å^{-1}$ correspond to the symmetry-related coincident reflections $\{1,1\}$ and $\{1,\bar{1}\}$ and to the $\{0,2\}$ reflection, respectively, of a rectangular unit cell containing two molecules with dimensions a = 4.93 Å and b = 7.43 Å and an area per molecule $ab/2$ of 18.3 $Å^2$. A weak $\{1,0\}$ reflection at q_{xy} = 1.27 $Å^{-1}$ and several high order reflections were also observed (*16–18*). Intensities of the Bragg rods of the two primary reflections $\{1,1\}$ + $\{1,\bar{1}\}$ and $\{0,2\}$ (Fig. 2) have maxima at q_z = 0, indicating that the molecules are vertical (*5, 19*). The unit cell dimensions are a fingerprint for the packing of hydrocarbon chains in the "orthogonal" mo-

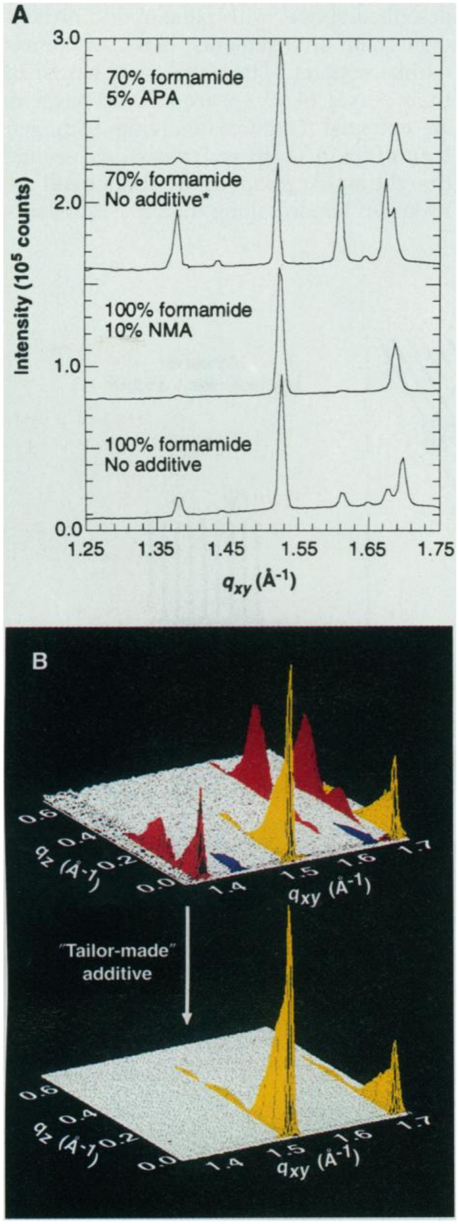

Fig. 1. (**A**) Grazing incidence x-ray diffraction patterns for arachidamide. All measurements gave approximately the same background level but have been offset in the vertical direction for clarity. For each value of q_{xy}, the measured intensity has been integrated over the entire q_z window, $0.0 \leq q_z \leq 0.8$ $Å^{-1}$. The subphase and additives (APA, 3-arachidamidopropionamide; NMA, *N*-methylarachidamide) are indicated above each curve. The measurement marked with an asterisk was carried out at ESRF, Grenoble; all others were carried out at HASYLAB, DESY, Hamburg. (**B**) Two-dimensional intensity distributions of the diffraction pattern of (top) arachidamide and (bottom) arachidamide containing 5% APA on 70 mol% formamide subphase as a function of the horizontal (q_{xy}) and vertical (q_z) scattering vectors. The reflections corresponding to each crystalline phase are shown in different colors: orthogonal in red, parallel in yellow, and minor phase in purple. The parallel phase is present primarily as a multilayer without additive but is primarily a monolayer when additive is present.

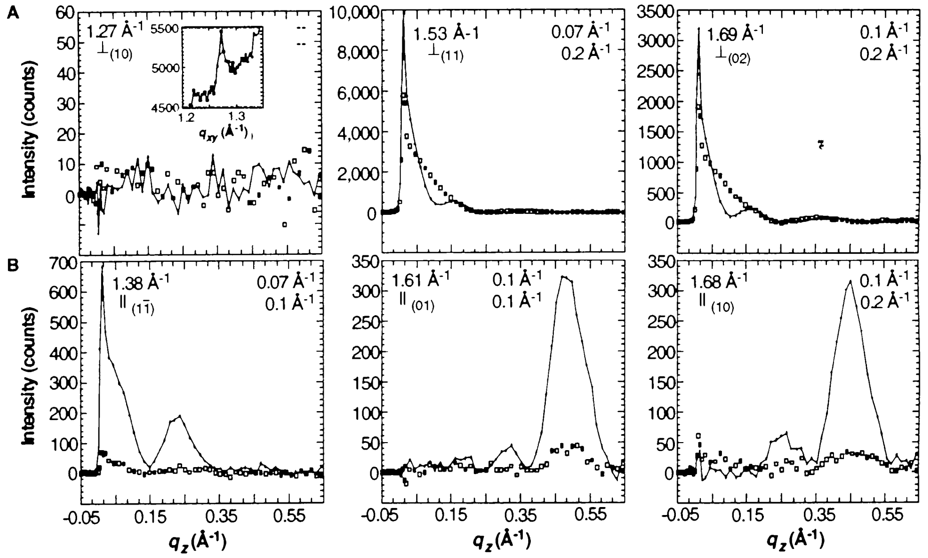

Fig. 2. Intensity profiles along the Bragg rods (*13, 14*) of the two major phases found for uncompressed pure arachidamide (solid line) and arachidamide containing 10% NMA (squares) on pure formamide subphase at 5° ± 1°C. (**A**) Phase with orthogonal chain packing. (**Inset**) Bragg peak along q_{xy} (integrated over q_z) for the first reflection. (**B**) Phase with parallel chain packing. The data were smoothed by averaging consecutive data points in sets of three. The observed position in q_{xy}, the $\{h,k\}$ assignment, and the structural arrangement of the chains (that is, parallel ∥ or orthogonal ⊥) for each Bragg peak are given on the left side, and the approximate FWHM of each Bragg rod on the right side (pure arachidamide, above; with additive, below). When the peak of the Bragg rod occurs at q_z = 0, data can only be obtained for the one-half of the Bragg rod with q_z > 0. The indicated FWHM for those Bragg rods that have their maxima at q_z = 0 have been doubled accordingly. Also, the innermost data points in the vicinity of q_z = 0 have a significantly enhanced intensity because of an interference phenomenon known as the Vineyard peak (*5, 13, 14*).

tif (Fig. 4A) in which the two molecules in the unit cell are related by glide symmetry, such that the hydrocarbon chains make herringbone contacts along the glide with a dihedral angle of about 90° between their planes (*6*). The length of the *a* axis is appropriate for hydrogen bonding between amide groups, suggesting that these groups are twisted out of the plane of the hydrocarbon chains so as to be approximately parallel to the *a* axis.

The second trilayer phase has three primary low order reflections, at q_{xy} = 1.38, 1.61, and 1.68 $Å^{-1}$, which were assigned, respectively, as the $\{1,\bar{1}\}$, $\{0,1\}$, and $\{1,0\}$ reflections, yielding an oblique unit cell with dimensions a = 4.92 Å and b = 5.13 Å, γ = 130.5°, and an area per molecule $ab\sin\gamma$ of 19.2 $Å^2$ (*8*, *20*, *21*). It is likely that N–H···O hydrogen bonding occurs parallel to one of the unit cell axes, because both are the right length for this interaction. The maximum intensity of the Bragg rod profile for the $\{1,\bar{1}\}$ reflection is at q_z = 0, and those of the other two reflections are at q_z = 0.46 $Å^{-1}$ (Fig. 2). Here again, the width of the Bragg rod profiles indicates that this phase is a molecular trilayer. It can thus be concluded that the molecules are tilted parallel to the 4.2 Å long diagonal (**a** + **b**) axis, with a tilt of about 17° (*19*) from the normal to the liquid surface. This packing mode is known as parallel because of the arrangement of the hydrocarbon chains (*22*, *23*) (Fig. 4A).

Two additional weak reflections at q_{xy} = 1.44 and 1.65 Å were observed (Fig. 1) but could not readily be assigned. If these Bragg peaks are assumed to belong to a single phase with a rectangular unit cell, then two possibilities arise. If the reflections are assigned as the $\{1,1\}$ + $\{1,\bar{1}\}$ and the $\{0,2\}$, respectively, then the unit cell is of dimensions a = 5.31 Å and b = 7.62 Å. If the assignments are reversed, then the calculated dimensions are a = 4.24 Å and b = 8.72 Å.

It is possible that the two major phases described above, with parallel and orthogonal chain arrangements, make an epitaxial-like contact. The equality in length of their *a* axes (4.93 versus 4.92 Å) suggests an epitaxial contact involving hydrogen bonds (Fig. 6A). In such a case, we assume that the amide groups in the oblique cell are hydrogen bonded along their *b* axes. A sec-

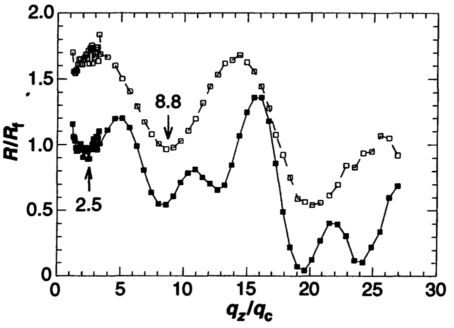

Fig. 3. Specular x-ray reflectivity curves for uncompressed arachidamide (■) and arachidamide containing 5% APA additive (□) (offset by 0.5 unit in R/R_f), over 70 mol% formamide subphase at 5° ± 2°C. The measured reflectivity divided by the Fresnel reflectivity, R/R_f, is calculated for a perfect, sharp interface; q_z/q_c is the normalized vertical scattering vector, where λ = 1.54 Å and q_c is the length of the scattering vector at the critical angle of incidence. The position of the first minimum in q_z/q_c is given for each curve. The lines are drawn to connect the data points.

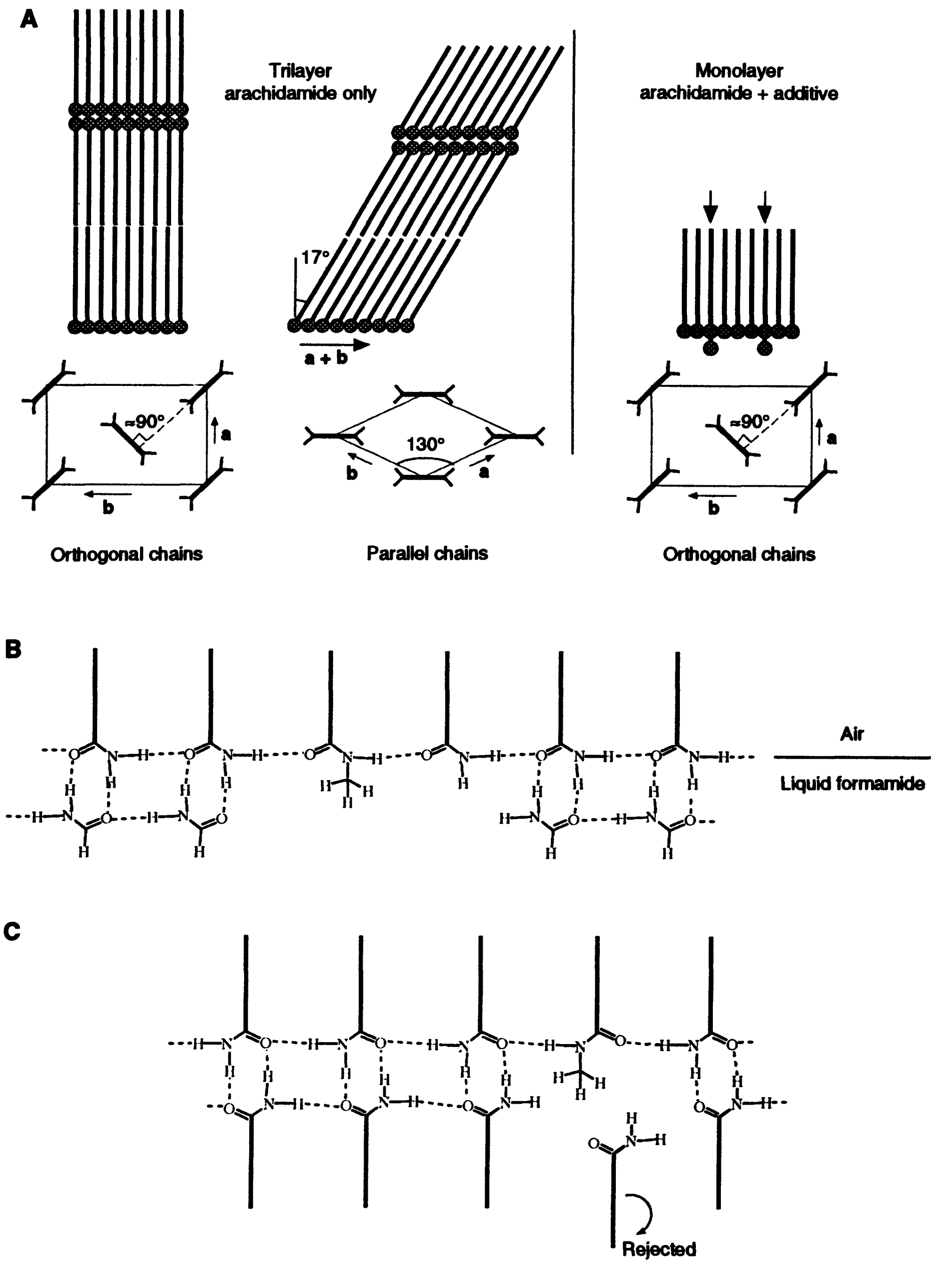

Fig. 4. (**A**) Schematic representation of the orthogonal and parallel packing arrangements of arachidamide molecules. (Bottom) Chain packing in the unit cells as viewed along the hydrocarbon chains. The thick black lines represent the projection of the hydrocarbon chains onto a plane perpendicular to the long molecular axis. (Top) Side view of monolayer and trilayer packing arrangements. Arrows indicate additive molecules. In the orthogonal arrangement, the molecules are approximately vertical with respect to the liquid surface. Chains packing in the parallel motif are tilted along the **a** + **b** diagonal. (**B** and **C**) Schematic representation of the effect of the additive NMA on the growth of arachidamide multilayer on formamide subphase: (B) The additional *N*-methyl group of the additive projects into the subphase but does not disrupt the intermolecular hydrogen bonding network within the monolayer; (C) bilayer cannot form because the *N*-methyl prevents bonding of an incoming amide group.

ond possibility is that the axes $\mathbf{a}_{\parallel} - \mathbf{b}_{\parallel}$ = 9.13 Å and $\mathbf{a}_{\perp} + \mathbf{b}_{\perp}$ = 8.93 Å line up (Fig. 6B). If such an epitaxy between the two phases does exist, it may be that domains of one phase serve as a template for growth of the other. The GID pattern of arachidamide (without additive) on formamide-water subphase was observed as a function of time, and a shift in the equilibrium between the two trilayers was observed (Fig. 5). It is also possible that the equilibrium occurs by dissolution of the peripheries of the crystalline domains and recrystallization in the second form.

Neither of these phases corresponds to the structure of 3D crystals of long-chain amides $C_nH_{2n+1}CONH_2$, where $n \leq 14$ (*24*). In these crystals, the hydrogen bonds within each layer are generated by glide symmetry with neighboring rows of highly tilted hydrocarbon chains tilted in opposite directions.

Auxiliary molecules were designed to inhibit multilayer formation while not disrupting growth within a layer. Two secondary amides, $C_{19}H_{39}CONHR$, where R = CH_3 [*N*-methylarachidamide (NMA)] or R = $C_2H_4CONH_2$ [3-arachidamidopropionamide (APA)], similar to arachidamide except for a bulky group attached to the amide nitrogen, were used as additives. When the amphiphilic material contains 5 to 10% of one of these auxiliaries, a single phase consisting of a monolayer is formed (*25*). The R groups of these molecules simply point into the liquid below (Fig. 4). In a multilayer, however, the additional bulky group prevents formation of the amide hydrogen bonded dimers in the overlying bilayer, thus inhibiting growth of the crystallite in the vertical direction. Such a selective inhibition of multilayer growth was indeed observed.

The GID patterns (Fig. 1) of arachidamide to which 5% APA or 10% NMA had been added before spreading on the subphase show primarily the two reflections associated with the orthogonal motif with the molecules aligned vertically (Fig. 4). The Bragg rods at high q_z, corresponding to the tilted structure found for arachidamide alone, are extrmely weak here, with only those corresponding to the orthogonal motif being observed (Fig. 1B). The FWHM of the Bragg rods for arachidamide plus additive are about two to three times those of the corresponding FWHM from pure arachidamide, indicating that the layer is about one-third as thick (Fig. 2) and is thus primarily monolayer. As can be seen from the low intensity of the Bragg rods corresponding to the tilted trilayer (Fig. 2B), only a small amount of this phase is present. There was no increase in the relative intensity of these reflections over the 3-hour duration of the experiment. It is not yet clear why the monolayer displaying the orthogonal motif with the molecules vertically aligned is preferred without appearance of a monolayer with parallel packing of tilted molecules. Molecules of triacontanoic acid in a monolayer, which are highly tilted over a water subphase, also align vertically on liquid formamide. This has been explained in terms of the hydrogen bonding network of bound formamide (*16*).

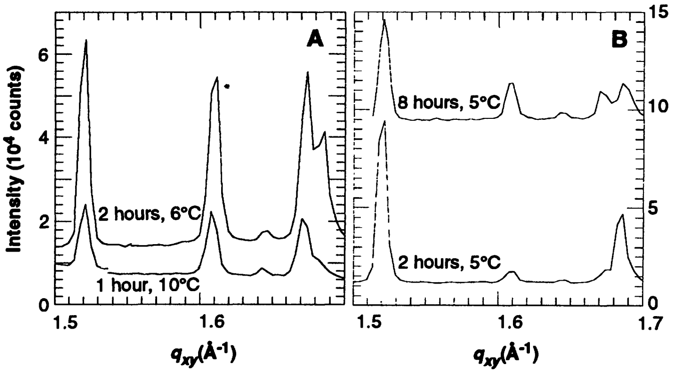

Fig. 5. GID patterns for arachidamide on 70 mol% formamide showing the change in the relative ratio of the two trilayer phases with time for two different experiments. The temperature and hours elapsed after spreading of the sample are indicated. (**A**) The first experiment, measured during cooling of the sample from room temperature to 5°C. (**B**) Second experiment, measurements begun after cooling to 5°C. The intensity measured after 8 hours has been multiplied by a factor of 12 to aid comparison by compensating for a decrease in the signal caused by radiation damage to the sample, and this curve has been offset in the vertical direction for clarity.

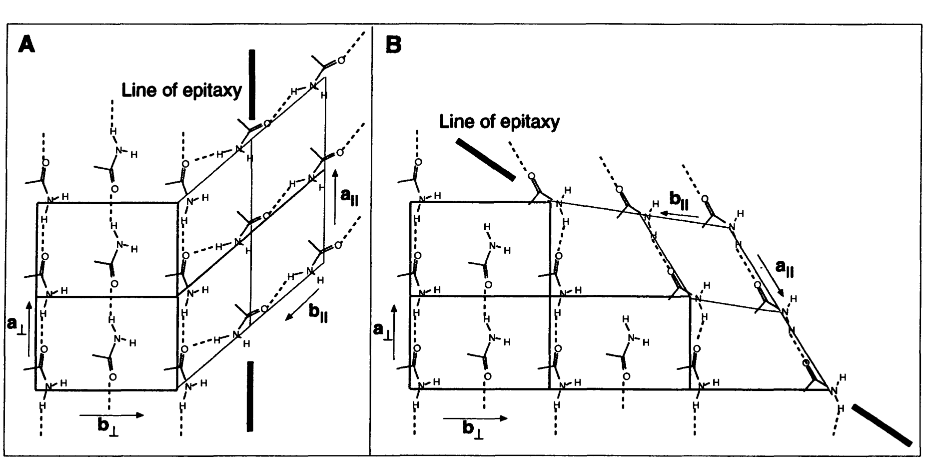

Fig. 6. Hydrogen bonding in two possible epitaxial contacts between the (**A**) orthogonal and (**B**) parallel packing modes. The symbols ∥ and ⊥ refer to parallel and orthogonal chain arrangements, respectively.

The effect of additive on arachidamide over 70 mol% formamide in water was also monitored with specular x-ray reflectivity. Measurements of arachidamide alone and arachidamide containing 5% APA are consistent with the formation of trilayer in the absence of additive but monolayer when it is present (Fig. 3). The position of the first minimum in the reflectivity curve for arachidamide plus contaminant is at about three times the value in q_z of that for arachidamide alone. The position of this minimum is, to a first approximation, inversely proportional to the thickness of the film (*15*), indicating that in the presence of additive, the film is roughly one-third as thick.

The coexistence of multiple phases in an amphiphilic system at the air-liquid interface may serve as a model for the early stages of 3D crystal nucleation in which a variety of nuclei representing different mature crystal phases may be present. Amphiphilic additives to the spreading solution have been shown to selectively influence "polymorphism" in these spontaneously formed, self-assembled crystalline thin films at the air-liquid interface. Selective inhibition by these additives influences the growth of the different coexisting nuclei, favoring the development of a single crystalline form. These results are in direct analogy to earlier studies in which tailor-made additives were used to influence the growth and morphology of 3D crystals (*1*, *26*, *27*) and suggest that tailor-made additives effect crystal growth at its earliest stages. A relevant example is that of crystallization of waxes in petroleum, where the morphology could be modified by use of long chain additives or solvents (*28*).

The choice of additive and subphase (*8*, *16*) may also be used to engineer the number of layers and the packing mode of thin films in a manner previously only available on solid support. These may have implications as models of biological membranes and in other applications. The observation of spontaneous multilayer formation suggests new ways for selective formation of multilayers versus monolayers, such as the use of molecules containing hydrophobic chains with hydrophilic groups at each end. The lateral and interlayer packing of these multilayers should be controllable through the use of amphiphilic tailor-made additives in a manner similar to that described in this report.

REFERENCES AND NOTES

1. I. Weissbuch, L. Addadi, M. Lahav, L. Leiserowitz, *Science* **253**, 637 (1991).
2. D. Zbaida *et al.*, *React. Polym.* **6**, 241 (1987).
3. E. Staab, L. Addadi, L. Leiserowitz, M. Lahav, *Adv. Mater.* **2**, 40 (1990).
4. The synchrotron radiation beam was monochromated to a wavelength of 1.35 Å at HASYLAB and 1.38 Å at ESRF. To maximize surface sensitivity, we adjusted the beam to strike the sample at an incident angle of $\alpha_f = 0.85\alpha_c$, where $\alpha_c \approx 0.14°$ is the critical angle for total external reflection. The dimensions of the incoming x-ray beam on the liquid surface were 50 mm by 2.5 mm. Several types of information are collected by the position sensitive detector (PSD), which has its axis along the vertical direction z. The scattered intensity measured by scanning different values of q_{xy} ($\approx 4\pi \sin\theta/\lambda$) and integrating over the whole q_z window of the PSD ($q_z = 2\pi \sin\alpha_f/\lambda$, where α_f is the angle between the water surface and the scattered beam) yields Bragg peaks. Because there is no selection rule or restriction along q_z, the GID patterns arise from a two-dimensional array of rods, called Bragg rods, which extend parallel to the vector q_z. The scattered intensity recorded in channels along the PSD but integrated in q_{xy} across a Bragg peak produces q_z-resolved scans called Bragg rod profiles. Schematic diagrams of the GID setup are given in (*5, 6*).
5. J. Als-Nielsen and K. Kjaer, in *Proceedings of the NATO Advanced Study Institute: Phase Transitions in Soft Condensed Matter*, T. Riste and D. Sherrington, Eds. (Plenum, New York, 1989), p. 113.
6. D. Jacquemain *et al.*, *Angew. Chem. Int. Ed. Engl.* **31**, 130 (1992), and references therein.
7. J. Als-Nielsen, in *Handbook on Synchrotron Radiation*, G. S. Brown and D. E. Moncton, Eds. (North-Holland, Amsterdam, 1991), vol. 3, pp. 471–503.
8. S. P. Weinbach *et al.*, *J. Am. Chem. Soc.* **115**, 11110 (1993).
9. Arachidic acid (Sigma; purity, 99%) was converted into arachidamide or NMA in two steps: the formation of the chloride derivative by action of $SOCl_2$ followed by treatment with ammonia for the primary amide or methylamine for the secondary amide. Purities were checked by thin layer chromatography. The identities of the compounds were checked by nuclear magnetic resonance and infrared spectroscopies. Spreading solutions were prepared in chloroform (Merck, analytical grade) with concentrations close to 5×10^{-4} M.
10. The correlation length, $L \approx 0.90 \times 2\pi/(\mathrm{FWHM}^2 - \Delta^2)^{1/2}$, where FWHM is the full width at half maximum of the Bragg peak and Δ is the resolution FWHM, associated with the GID $\{h,k\}$ reflection corresponds to the average length of all diffracting crystallites over which "perfect" crystallinity extends in the direction of the reciprocal lattice vector $\mathbf{d}^*_{hk}$.
11. A. Guinier, *X-ray Diffraction* (Freeman, San Francisco, CA, 1968).
12. The approximate thickness T of the crystalline film (in angstroms) is given by 0.9 $[2\pi/\mathrm{FWHM}(Q_z)]$, where $\mathrm{FWHM}(Q_z)$ is the FWHM of the Bragg rod in reciprocal angstroms.
13. The sharp peak observed at around $q_z = 0.01$ Å^{-1} is caused by the interference of rays diffracted up with rays diffracted down and subsequently reflected back up by the interface (*14*).
14. G. Vineyard, *Phys. Rev. B* **26**, 4146 (1982).
15. K. Kjaer, J. Als-Nielsen, C. A. Helm, P. Tippman-Krayer, H. Möhwald, *J. Phys. Chem.* **93**, 3200 (1989).
16. S. P. Weinbach, K. Kjaer, J. Als-Nielsen, M. Lahav, L. Leiserowitz, *ibid.* **97**, 5200 (1993).
17. Several high order reflections were also observed, although not all q_{xy} values were measured. Those found were the $\{1,2\} + \{1,\bar{2}\}$ ($q_{xy} = 2.11$ Å^{-1}), $\{2,0\}$ (2.53 Å^{-1}), $\{2,1\} + \{2,\bar{1}\}$ (2.67 Å^{-1}), and the $\{1,3\} + \{1,\bar{3}\}$ (2.85 Å^{-1}) reflections. The region of the $\{0,1\}$ reflection, calculated to be at $q_{xy} = 0.85$ Å^{-1}, was not measured.
18. During an earlier measurement at the bending magnet beamline (*16*), two reflections were observed for arachidamide over formamide. These were interpreted as a single phase composed of a trilayer with the molecules vertically oriented with respect to the liquid surface. Closer inspection of the earlier GID pattern reveals that the additional reflections were in fact present but were of such low intensity that they were not noticed.
19. The tilt, t, of the molecules is given by $\tan t \cos \Psi_{hk} = q_z^0/q_{hk}$, where q_z^0 is the maximum position of the Bragg rod along q_z, q_{hk} is the position of the hk reflection in q_{xy}, and Ψ_{hk} is the angle between the direction of tilt as projected onto the horizontal plane and the reciprocal lattice vector hk (*5*).
20. These dimensions are similar to those found for the diamide APA over water subphase (*8*).
21. The $\{2,1\} + \{2,\bar{1}\}$ ($q_{xy} = 2.49$ Å^{-1}) and $\{1,2\} + \{1,\bar{2}\}$ (2.61 Å^{-1}) reflections were also measured.
22. We may describe the structure in terms of the pseudorectangular cell $\mathbf{a}' = \mathbf{a} + \mathbf{b} = 4.21$ Å and $\mathbf{b}' = \mathbf{a} - \mathbf{b} = 9.13$ Å, with $\gamma' = 93.2°$. The unusually long $\mathbf{b}'$ axis is strongly indicative that the plane passing through the hydrocarbon backbone is parallel to the axis $\mathbf{b}'$ (Fig. 4), as has been seen in 3D crystal structures of α,ω-diamides (*23*). The chains of the two molecules in the unit cell are therefore likely to be parallel to one another. Thus, we may describe the structure in terms of the oblique unit cell $\mathbf{a},\mathbf{b},\gamma$ with one molecule per unit cell, and all molecules in the crystal are related by translation.
23. P. M. Hospital, *Acta Crystallogr. B* **27**, 484 (1971),
24. J. D. Turner and E. C. Lingafelter, *Acta Crystallogr.* **8**, 549 (1955); *ibid.*, p. 551.
25. A monolayer of amphiphilic molecules at the air-liquid interface may be regarded as a different phase than a multilayer with the same intralayer packing mode. A monolayer contains essentially three sets of intermolecular interactions, namely the intralayer interactions between molecules, the interaction between the polar head group and the subphase, and that of the terminal methyl with the air. The corresponding multilayer contains these same interactions plus two additional contacts: the interlayer head-to-head contacts between polar head groups and the interlayer contacts between terminal methyl groups.
26. L. Addadi *et al.*, *Angew. Chem. Int. Ed. Engl.* **24**, 466 (1985).
27. M. Lahav and L. Leiserowitz, *J. Phys. D* **26**, B22 (1993).
28. K. Lewtas, R. D. Tack, D. H. M. Beiny, J. W. Mullin, in *Advances in Industrial Crystallization*, J. Garside, R. J. Davey, A. G. Jones, Eds. (Butterworth-Heinemann, Oxford, 1991), p. 166.

29. We thank E. Shavit for the syntheses of the additive materials and F. Leveiller and D. Jacquemain for assistance with the GID measurements. We acknowledge financial support from The Minerva Foundation, Munich, the Israel Academy of Science and Humanities, and the Danish Foundation for Natural Sciences. We also acknowledge HASYLAB, DESY, Hamburg, and ESRF, Grenoble, for beam time.

24 January 1994; accepted 14 April 1994

New Phases of C_{60} Synthesized at High Pressure

Y. Iwasa,* T. Arima, R. M. Fleming, T. Siegrist, O. Zhou,
R. C. Haddon, L. J. Rothberg, K. B. Lyons, H. L. Carter Jr.,
A. F. Hebard, R. Tycko, G. Dabbagh, J. J. Krajewski,
G. A. Thomas, T. Yagi

The fullerene C_{60} can be converted into two different structures by high pressure and temperature. They are metastable and revert to pristine C_{60} on reheating to 300°C at ambient pressure. For synthesis temperatures between 300° and 400°C and pressures of 5 gigapascals, a nominal face-centered-cubic structure is produced with a lattice parameter $a_o = 13.6$ angstroms. When treated at 500° to 800°C at the same pressure, C_{60} transforms into a rhombohedral structure with hexagonal lattice parameters of $a_o = 9.22$ angstroms and $c_o = 24.6$ angstroms. The intermolecular distance is small enough that a chemical bond can form, in accord with the reduced solubility of the pressure-induced phases. Infrared, Raman, and nuclear magnetic resonance studies show a drastic reduction of icosahedral symmetry, as might occur if the C_{60} molecules are linked.

Although C_{60} molecules are extremely stable at ambient conditions, nonhydrostatic compression induces a transformation of C_{60} to diamond (*1*) or unknown structures above 15 GPa (*2–4*). Light irradiation is also reported to cause a polymerization (*5*). We have found at least two crystalline phases of carbon involving crosslinked C_{60} cages that can be synthesized from pure C_{60}.

Synthesis was performed at high pressure and high temperature with a wedge-type cubic anvil apparatus (*6*), which produces quasi-hydrostatic pressure. About 20 mg of C_{60} was pressed into a pellet and sandwiched between two Ti-powder oxygen get-

---

Y. Iwasa, R. M. Fleming, T. Siegrist, O. Zhou, R. C. Haddon, L. J. Rothberg, K. B. Lyons, H. L. Carter Jr., A. F. Hebard, R. Tycko, G. Dabbagh, J. J. Krajewski, G. A. Thomas, AT&T Bell Laboratories, Murray Hill, NJ 07974, USA.
T. Arima, Department of Physics, University of Tokyo, Tokyo 113, Japan.
T. Yagi, Institute for Solid State Physics, University of Tokyo, Tokyo 106, Japan.

*On leave from the Department of Applied Physics, University of Tokyo, Tokyo 113, Japan.